Effect of Beta Shear on Simulated Tropical Cyclones

JUAN FANG

Key Laboratory of Mesoscale Severe Weather (MOE), College of Atmospheric Sciences, Nanjing University, Nanjing, China

FUQING ZHANG

Department of Meteorology, The Pennsylvania State University, University Park, Pennsylvania

(Manuscript received 25 October 2010, in final form 12 April 2012)

ABSTRACT

Through cloud-resolving simulations, this study examines the effect of β on the evolution of tropical cyclones (TCs). It is found that the TC simulated on a β plane with variable Coriolis parameter f is weaker in intensity but larger in size and strength than the TC simulated on an f plane with constant f. Such differences result mainly from the effect of the β shear rather than from the variation of f due to the latitudinal change of the TC position, as illustrated in a three-stage conceptual model developed herein. The first stage begins with the establishment of the β shear and the emergence of asymmetries as the TC intensifies. The β shear peaks in value during the second stage that subsequently leads to the formation of an extensive stratiform region outside of the primary eyewall. The evaporative cooling associated with the stratiform precipitation acts to sharpen the low-level equivalent potential temperature gradient into a frontlike zone outside of the eyewall region, which leads to the burst of convection outside of the primary eyewall. The third stage is characterized by a weakening β shear and the corresponding TC vortex axisymmetrization and expansion. The convection on the inner edge of the stratiform region becomes more organized in the azimuthal direction and eventually causes the TC structure to evolve in a manner similar to the secondary eyewall formation and eyewall replacement usually observed in TCs. It is the active convection outside of the primary eyewall that contributes to a relatively weaker but larger TC on the β plane than that on the f plane.

1. Introduction

As the tropical cyclone (TC) evolves in an environment with variable planetary vorticity (i.e., on a β plane), the so-called β gyres are produced through the advection of planetary vorticity by the storm-scale cyclonic circulation. This advection leads to the development of regions of anomalously low and high vorticity northeast and southwest of the cyclone center, respectively (Holland 1983). Such a wavenumber-1 asymmetry associated with the β gyres plays an important role in the evolution of TCs, which have been extensively studied for decades.

With two-dimensional models, it is found that the asymmetric gyres lead to a relative flow across the vortex core that causes it to propagate poleward and westward (i.e., β drift; e.g., Chan and Williams 1987; Fiorino and Elsberry 1989; Carr and Williams 1989). Wang and Holland (1996a,b) further pointed out that the relative flow across the vortex core varies with height and leads to the tilting of the cyclonic vortex and the shearing of the upper anticyclonic circulation. This in turn can modify the speed of the poleward and westward motion of the TC via the interaction between the low- and upper-level circulations of the tilted vortex.

Although it is well understood that the β effect may influence the movement of TCs, there is less consensus on the impact of the β effect on the intensity of TCs. Madala and Piacsek (1975) found that a vortex on a β plane may intensify at a slower rate than the one on an f plane (i.e., with constant planetary vorticity, f) before the storm stage, but at the same rate thereafter. DeMaria and Schubert (1984) showed that the intensification rates for simulations on an f plane and a β plane were similar until 48 h; afterward, the intensity of the storm on the f plane continued to increase, while the storm on the β plane began to level off. They attributed such a difference to a larger inertial stability in the upper layer and the vertical

Corresponding author address: Dr. Fuqing Zhang, Department of Meteorology, The Pennsylvania State University, University Park, PA 16801.
E-mail: fzhang@psu.edu

DOI: 10.1175/MWR-D-10-05021.1

shearing of the centers in the β-plane simulation. Similar evolution of the TC vortex on a β plane was reproduced in Peng et al. (1999), Wu and Braun (2004), and Kwok and Chan (2005), but with different interpretations. Peng et al. (1999) suggested that the β effect may lead to a phase shift between the maxima of the asymmetric moisture convergence and surface fluxes, which could reduce precipitation and inhibit the TC development. Wu and Braun (2004) indicated that the eddy momentum fluxes associated with the asymmetries induced by the β effect weakens the tangential and radial flows of the mean TC circulation. Kwok and Chan (2005) ascribed the relatively weak TC development on the β plane to the vertical wind shear caused by the β effect. Different from the aforementioned works, some recent studies suggest that TCs are not significantly affected by the β effect. For example, Ritchie and Frank (2007) found that the difference in minimum pressure between the TCs on an f plane and a β plane is never more than 10 hPa throughout their 72 h of simulation. Similar conclusions can also be found in Liang and Chan (2005) and Nguyen et al. (2008). Nguyen et al. (2008) speculated that some of the β effect on TCs in previous studies could be an artifact of considerably coarser horizontal resolution and parameterized convection used in their TC simulations [e.g., 15 km in Kwok and Chan (2005); 25 km in Wu and Braun (2004); 0.5° in Peng et al. (1999)].

The influence of the β effect on TC structure has also been discussed extensively in literature. Bender (1997) pointed out that the vorticity advection due to differences between the low-level β-gyre flow and the storm motion induces quasi-steady asymmetries in the eyewall region, responsible for the asymmetric structure in the upward motion and accumulated precipitation with a corresponding maximum in the rear quadrant of the eyewall. Ritchie and Frank (2007) found that, when a variable-f environment is imposed on a mature TC, a persistent north-northwesterly vertical wind shear develops over the storm center, and causes the development of a persistent wavenumber-1 asymmetry in the inner-core structure with upward motion and rainfall concentrated in the downshear-left region. The vertical wind shear that resulted from the height-varied advection of the planetary vorticity was termed the "β shear" by Ritchie and Frank (2007). With high-resolution simulations of TCs in environments with constant and variable Coriolis parameters, Wang (2006) found that, in addition to the introduction of asymmetric structure in inner core, the β effect contributes to the occurrence of concentric eyewalls, subsequent eyewall replacement, and the associated intensity change. He proposed that the β effect modifies the radial potential vorticity (PV) structure of the TC and produces a constant asymmetric forcing for the generation of convective spiral rainbands, which are favorable for the development of a quasi-annular rainband.

The primary objective of the current study is to reexamine the evolution of the TC embedded in an environment with variable planetary vorticity in the viewpoint of the influence of the β shear on TCs following the work of Ritchie and Frank (2007) and Wang (2006). Section 2 presents the model configuration and experimental design. Section 3 contains an overview of simulated TC intensity and size, while sections 4 and 5 discuss the evolution of the β shear and its effect on the TC structure, respectively. In section 6, a schematic illustration of the evolution of a TC on a β plane is presented. A summary is provided in section 7.

2. Model configuration and experimental design

This study uses the Weather Research and Forecasting Model (WRF) version 2.2 (Skamarock et al. 2005). The model contains two domains with horizontal grid spacing of 9 and 3 km and domain sizes of 10 800 km by 10 800 km and 3000 km by 3000 km, respectively. Two-way interactive nesting is used with the nested domain automatically moving to follow the model TC. The model has 35 levels in the vertical with the model top at ~28 km. Considering that the finer domain is large enough to cover the convection in the inner-core area and outer spiral rainbands, cumulus parameterization is not adopted even on the coarse mesh in this study. In addition, the use of a radiative parameterization is avoided with the intention to retard the growth of convection on the outer grid following Nolan (2007). The WRF Single-Moment 6-Class Microphysics scheme (WSM6) with graupel (Hong et al. 2004) and the Yonsei University (YSU) planetary boundary layer (PBL) scheme (Noh et al. 2003) are used in the simulations.

Simulation "EXP-f" is initialized with an axisymmetric cyclonic vortex similar to that used by Rotunno and Emanuel (1987) on an f plane at 20°N in a quiescent environment over the ocean with a constant sea surface temperature of 29.15°C. The initial thermodynamic structure of the unperturbed model atmosphere is defined as the Jordan mean hurricane season sounding for the Caribbean (Jordan 1958). The initial baroclinic vortex is in gradient-wind balance with the maximum winds of 16 m s^{-1} at a radius of ~102 km, equivalent to a strong tropical depression.

Simulation "EXP-β" is similar to EXP-f except for being performed on a β plane with the initial vortex centered at 20°N with variable Coriolis parameter:

$$f = f_c + \beta y, \tag{1}$$

where f_c, β, and y are the Coriolis parameter at the storm center, the gradient of the planetary vorticity, and the distance from the storm center in the north–south direction, respectively. Obviously, the TC simulated in EXP-β is influenced by the variation of f_c as the storm moves poleward and the meridional gradient of the Coriolis parameter across the TC circulation (i.e., the β effect). To separate the impact due to the variation of f_c from that due to the β effect, simulation "EXP-f_c" is conducted by neglecting the βy term in Eq. (1), while the Coriolis parameter f of the entire model domain is updated at every time step with the value at the storm center derived from EXP-β (i.e., $f = f_c$). To carry out EXP-f_c, the storm center of the simulated TC in EXP-β is saved every hour and then linearly interpolated to obtain the values of f_c at every time step.

3. Sensitivity of TC track, intensity, strength, and size to the beta effect

The simulations show the TC developed in EXP-β takes a northwest track, while the center (defined by the location of minimum sea level pressure) of the TCs in both EXP-f and EXP-f_c remains near their initial positions (not shown). In the first 96 h, the model TC in EXP-β moves northwestward with a speed of ~1.35 m s^{-1} (0.68 m s^{-1} westward and 1.17 m s^{-1} northward) while, after 96 h, the motion is more poleward but less westward with a speed of ~2.38 m s^{-1} (0.85 m s^{-1} westward and 2.22 m s^{-1} northward). Both speeds are comparable with those found in Wang and Holland (1996a) and Bender (1997). The change of motion that occurred near 96 h is also in agreement with the findings of Wang and Holland (1996a,b), who argued that the change is associated with an upper-level anticyclone that developed to the south of the low-level vortex.

Following Holland and Merrill (1984), the TC intensity, strength and size are defined by the maximum surface (10 m) azimuthal wind speed ("maxWSP") and the minimum sea level pressure ("minSLP"), the average relative angular momentum of the surface circulation inside the 300-km radius, and the axisymmetric extent of hurricane force winds (33 m s^{-1}), respectively. Figure 1 shows the time evolutions of the TC intensity, strength, and size for all three experiments. After a short period of initial spinup, the model TCs intensify gradually in all experiments. As in Nguyen et al. (2008), there is little difference in the evolution of minSLP and maxWSP among the three simulations in the first 88 h of integration (Fig. 1a). Afterward, the simulated TCs in EXP-f and EXP-f_c become more intense than that in EXP-β and finally reach a peak intensity of ~910 hPa for minSLP and ~60 m s^{-1} for maxWSP at ~168 h, about 15 hPa lower in minSLP and 8 m s^{-1} stronger in maxWSP than those in EXP-β (Fig. 1a). Such intensity differences are noticeably larger than those reported by Ritchie and Frank (2007), primarily because their simulations were integrated for only 72 h before the larger differences emerge. The intensity differences are nevertheless smaller than those obtained by Kwok and Chan (2005), likely due to their use of a coarser grid spacing (15 km) with parameterized convection.

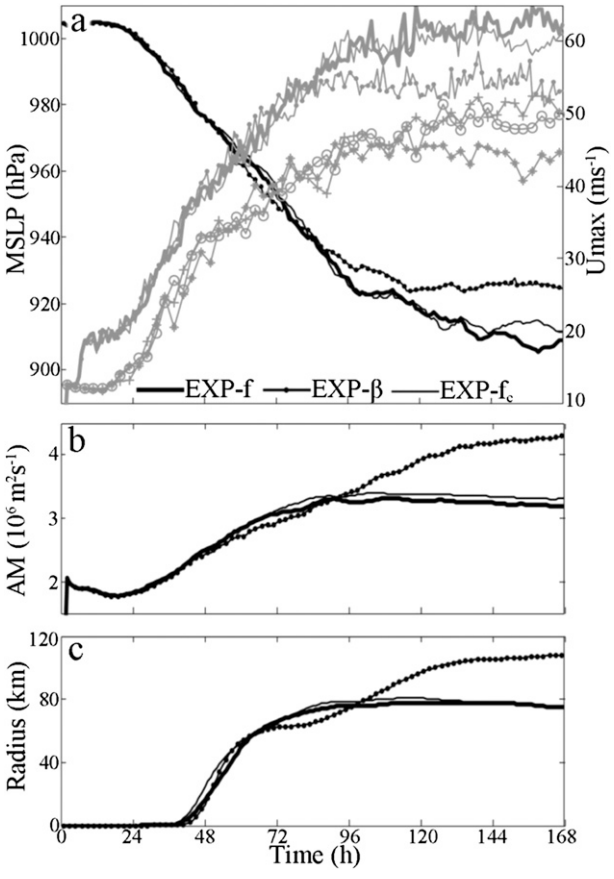

FIG. 1. Time evolutions of (a) the intensity in terms of minimum sea level pressure (black) and maximum 10-m wind speed (gray), (b) strength, and (c) size for the simulated TCs in EXP-f (thick solid line), EXP-f_c (thin solid line), and EXP-β (line with solid circle). The gray lines with "+," "o," and "★" denote the azimuthal-mean tangential wind at $z = 10$ m for the simulated TCs in EXP-f, EXP-f_c, and EXP-β, respectively.

Similar to intensity, the differences of the TC strength and size between EXP-f and EXP-f_c are much smaller than that between EXP-f and EXP-β after about 88 h (Figs. 1b,c). The average relative angular momentum of the surface circulation inside the 300-km radius and the radius of the azimuthal-mean tangential wind of 33 m s^{-1} in EXP-β are about 1.1×10^6 m^2 s^{-1} and 35 km greater than that of the other cases at the end of the simulations. Since the initial fields are identical in EXP-f and EXP-β except for the different f, the differences in TC intensity, strength, and size between these two experiments could

not have come from initial differences in synoptic environment (Merrill 1984), environmental moisture distribution (Wang 2009; Hill and Lackmann 2009), or the initial vortex sizes (Xu and Wang 2010a). Also, resemblance of EXP-f_c to EXP-f indicates that the latitudinal changes induced by the poleward motion of TCs cannot explain the differences in intensity, strength, and size between EXP-f and EXP-β. Therefore, the β effect is more important to the TC intensity, strength, and size than the variation of f_c.

The differences in TC intensity and size between EXP-β and EXP-f may have come from asymmetries in TC convection induced by the β effect. Previous studies have shown that the intensity and size of a TC are closely related to convection and its distribution (e.g., Xu and Wang 2010a,b; Wang 2009; Hill and Lackmann 2009; Hack and Schubert 1986). Figure 2 shows the plan view of the model-derived reflectivity at 96 and 114 h and the radial distribution of the azimuthal-mean tangential velocity at $z = 3$ km at 109, 113, 115, and 118 h in EXP-f and EXP-β. The most noticeable differences indicated by Figs. 2a–d are that the convection outside of the eyewall is more widespread and vigorous in EXP-β than that in EXP-f. From Figs. 2d,f we can see that a well-organized convective ring, accompanied by a secondary maximum in the azimuthal-mean tangential velocity, develops in the area beyond the eyewall in EXP-β at $t = 114$ h. The fact that the secondary convective ring can form on a β plane, while failing to develop on an f plane with the similar model settings was first noted by Wang (2006). He proposed that the asymmetric forcing exerted by the β effect activates the stratiform processes and leads to the enhancement of midlevel PV, which plays a critical role in the formation of the secondary convective band outside of the eyewall. The following sections examine the development of beta shear and the associated active convection outside of the eyewall in EXP-β in detail with the focus on the contribution of the low-level thermal contrast induced by the stratiform processes. The roles of an expanding wind field and inertial stability in the secondary eyewall formation will be presented in a companion study of Rozoff et al. (2012).

4. Development and evolution of the β shear

As a variable-f environment is applied to a baroclinic TC-like vortex, the β shear develops (Ritchie and Frank 2007; Kwok and Chan 2005; Bender 1997; DeMaria and Schubert 1984). Bender (1997) suggested that the β gyres can contribute up to $\sim$5 m s^{-1} of vertical wind shear. Ritchie and Frank (2007) found the β shear between 850 and 200 hPa can be stronger than 8 m s^{-1}. However, they speculated that this value is likely due to some instability in the outflow layer of the model TC and is unrealistic. In this section, the evolution of the β shear will be examined in detail. Since the differences between EXP-f and EXP-f_c in intensity and size are small, experiment EXP-f_c will not be examined any further.

As in Zehr (2003), the vertical wind shear is defined as $(\mathbf{V}_{12\text{km}} - \mathbf{V}_{1.5\text{km}})$, where $\mathbf{V}_{12\text{km}}$ and $\mathbf{V}_{1.5\text{km}}$ are the averaged environmental wind calculated for the annulus with radii at 200 and 800 km surrounding the vortex center at $z = 12$ and 1.5 km, respectively. Figure 3a shows the time evolution of the vertical wind shear obtained in EXP-f and EXP-β. The shear imposed on the TC in EXP-f is weak and stays below 1 m s^{-1} throughout the integration. In contrast, the shear increases continuously to 8.2 m s^{-1} in the first 88 h of integration and then decreases gradually in EXP-β. The peak value of 8.2 m s^{-1} is larger than that of Bender (1997) but comparable to Ritchie and Frank (2007). Along with the changes in magnitude, the direction of the shear backs cyclonically from the north-northeast to southwest in EXP-β (Fig. 3b). The significant rotation occurs in the period from 36 to 72 h and 128 to 168 h while some small cyclonic rotation of the shear can be identified in the period from $t = 72$ to 115 h.

Figure 3 also shows that the β-shear variation results mainly from changes in the wavenumber-1 component of the flow, mostly due to the asymmetric flow at the upper levels, (i.e., $\mathbf{V}_{12\text{km}}$). As shown in Fig. 4, and consistent with Wang and Holland (1996b), the increase and decrease of $\mathbf{V}_{12\text{km}}$ before and after 88 h and the cyclonic rotation of $\mathbf{V}_{12\text{km}}$ shown in Fig. 3 are closely related to the variation in the wavenumber-1 vorticity field. In the first 72 h (Figs. 4a–c), the positive (negative) vorticity band spiraling outward anticyclonically from the northwest (southeast) quadrant of the TC with the strongest vorticity perturbations lying in the north-northwest (south southeast) side of the TC outskirts develops gradually. Accordingly, a pair of counter-rotating β gyres emerges at the far northeast and southwest sides of the TC. The gyres introduce northwesterly flow over the TC inner area at radii smaller than 800 km (Figs. 4c,d and 3b). The enhanced northwesterly flow results in a peak β shear of approximately 8.2 m s^{-1} shortly before 96 h (Figs. 3 and 4d).

After 96 h (Figs. 4d–f), the wavenumber-1 vorticity pattern in the upper levels presents noticeable cyclonic rotation with considerable enhancement of the positive (negative) vorticity in the southwest (northeast) quadrant of the annulus between 300 and 900 km. Concurrently, the cyclonic (anticyclonic) gyre located in the far northeast (southwest) quadrant of the TC shifts outward and eventually moves out of the domain of interest. Consistently, the northwesterly flow decays and is gradually replaced by a southerly flow in the upper layer of the TC. The weakening of the mean velocity averaged in the annulus with radii from 200 to 800 km leads to a significant reduction of the β shear (Fig. 3b). Figures 4c–f also shows that the winds

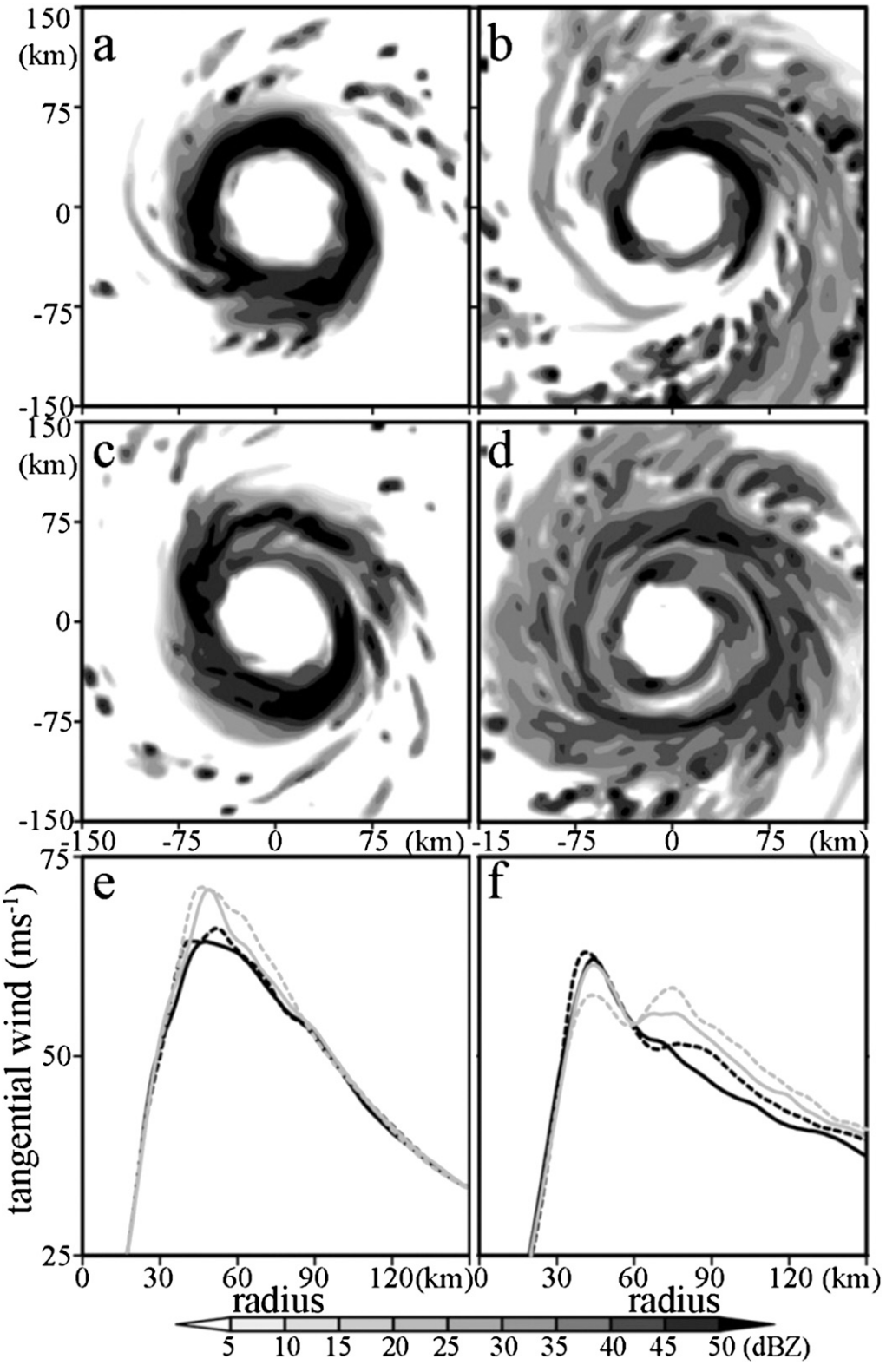

FIG. 2. Plan view of the model-derived reflectivity at $z = 4$ km at 96 h in (a) EXP-f and (b) EXP-β. (c),(d) As in (a),(b), but for 114 h. Radial variation of the azimuthal-mean tangential velocity at $z = 3$ km at 109 (black solid line), 113 (black dashed line), 115 (gray solid line), and 118 h (gray dashed line) in (e) EXP-f and (f) EXP-β.

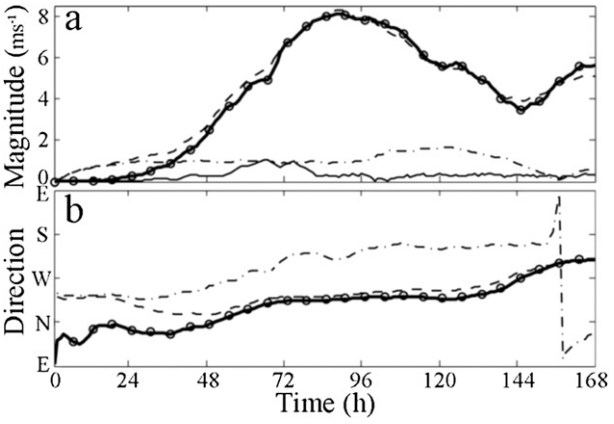

FIG. 3. (a) Time evolutions of the vertical wind shear magnitude between $z = 1.5$ and 12 km in EXP-f (thin line) and EXP-β (thick line). The dash–dotted and dashed lines denote the area-mean horizontal velocities of wavenumber-1 component at $z = 1.5$ and 12 km in EXP-β, respectively. (b) Time evolutions of the directions of the shear (solid), area-mean horizontal winds (storm-relative) at $z = 1.5$ km (dashed–dotted) and 12 km (dashed) in EXP-β. The "o"s in (a) and (b) denote the magnitude and direction of the shear induced by the wavenumber-1 component every 6 h in EXP-β.

are distinctly diverted around the TC central area with radius smaller than 200 km. This indicates that, in addition to the cyclonic rotation of the wavenumber-1 vorticity pattern, the stiffening of the TC vortex as it intensifies may have also contributed to the variation of the upper-level flow over the TC central area as proposed in Willoughby et al. (1984), Jones (1995), and Reasor et al. (2004).

To further understand the evolution of the upper-level wavenumber-1 vorticity field, prevailing flow, and the β shear, a vorticity budget analysis is conducted. The vorticity equation in the reference frame translating with the TC motion can be written as

$$\frac{\partial \zeta}{\partial t} = -\mathbf{V}_h \cdot \nabla_h \zeta - w\frac{\partial \zeta}{\partial z} - \beta v - (f_c + \beta y + \zeta)\nabla_h \cdot \mathbf{V}_h - \mathbf{k} \cdot \left(\nabla_h w \times \frac{\partial \mathbf{V}_h}{\partial z}\right) - \mathbf{k} \cdot (\nabla_h \alpha \times \nabla_h p) + \mathbf{k} \cdot (\nabla \times \mathbf{F}), \tag{2}$$

where ζ is the vertical component of relative vorticity and $\mathbf{V}$, α, p, and $\mathbf{F}$ are storm-relative velocity, specific volume, pressure, and friction, respectively. The subscripts "h" denote the horizontal component. Via decomposition of each variable in Eq. (2) as $A = \overline{A} + A'$, where the quantities with overbar and prime are the symmetric and asymmetric components, respectively, and subtracting the azimuthal mean vorticity tendency equation from Eq. (2), a vorticity tendency equation for the wavenumber-1 component can be obtained (after wavenumber decomposition) as

$$\frac{\partial \zeta_1}{\partial t} = \underbrace{-\overline{\mathbf{V}}_h \cdot \nabla_h \zeta_1}_{\text{HADV}_s} \underbrace{-\mathbf{V}_{h1} \cdot \nabla_h \overline{\zeta}}_{\text{HADV}_1} \underbrace{-(\mathbf{V}_h' \cdot \nabla_h \zeta')_1}_{\text{HADV}_n} \underbrace{-\beta \overline{v}}_{\text{BETA}} \underbrace{-\left(\overline{w}\frac{\partial \zeta'}{\partial z} + w'\frac{\partial \overline{\zeta}}{\partial z} + w'\frac{\partial \zeta'}{\partial z}\right)_1}_{\text{WADV}} \underbrace{-[(f_c + \overline{\zeta})\nabla_h \cdot \mathbf{V}_h' - (\beta y + \zeta')\nabla_h \cdot \overline{\mathbf{V}}_h - (\beta y + \zeta')\nabla_h \cdot \mathbf{V}_h']_1}_{\text{DIV}} \underbrace{-\mathbf{k} \cdot \left(\nabla_h \overline{w} \times \frac{\partial \mathbf{V}_h'}{\partial z} + \nabla_h w' \times \frac{\partial \overline{\mathbf{V}}_h}{\partial z} + \nabla_h w' \times \frac{\partial \mathbf{V}_h'}{\partial z}\right)_1}_{\text{TILT}}, \tag{3}$$

where the subscripts "1" denote the wavenumber-1 component of the related variables. The terms on the right-hand side of Eq. (3) represent contributions to the change of ζ_1 due to horizontal advection of ζ_1 by the symmetric flow (HADV_s), horizontal advection of $\overline{\zeta}$ by the wavenumber-1 component of the flow (HADV_1), horizontal advection related to nonlinear interactions among the asymmetric perturbations (HADV_n), the β effect (BETA), vertical advection (WADV), stretching (DIV), and titling (TILT), respectively. For simplicity, the solenoidal and subgrid-scale terms have been omitted in Eq. (3) because of their small contribution to the net vorticity tendency (Montgomery et al. 2006).

Figure 5 gives the 12-km wavenumber-1 vorticity tendency produced by the β effect, horizontal and vertical advection, stretching, and tilting averaged over the first 96 h. Although the asymmetry is initially induced by the β effect, the wavenumber-1 vorticity with the strongest vorticity perturbations on the north-northwest (south-southeast) side of the TC outskirts is mainly produced by the horizontal advection (Figs. 5a–c). Because of the horizontal advection of $\overline{\zeta}$ by the wavenumber-1 component of the flow, the positive and negative vorticity anomalies are strengthened in the northwest and southeast quadrants of the TC, respectively (Fig. 5d). Meanwhile, the positive (negative) vorticity produced by HADV_1 to the northwest (southeast) of the TC outer

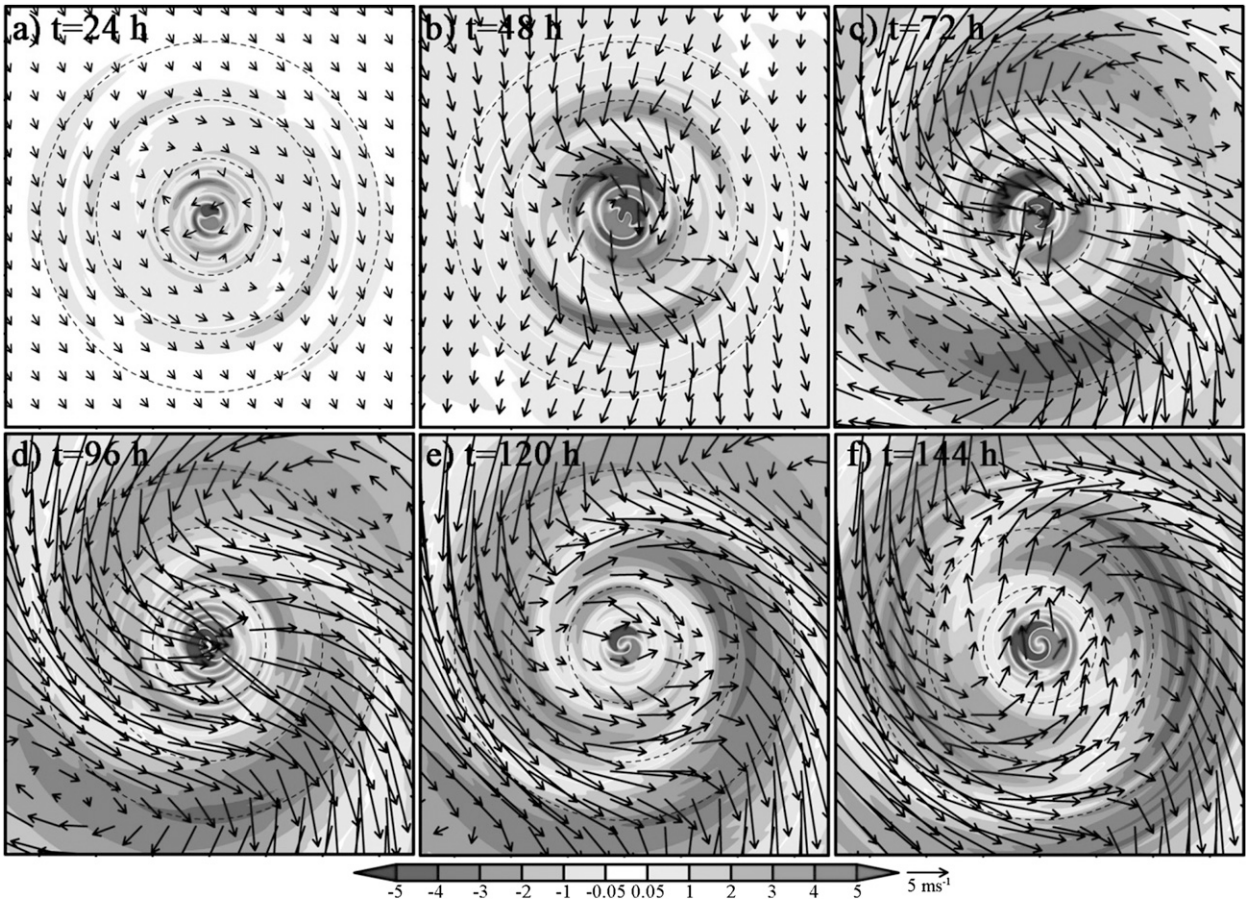

FIG. 4. The 12-km storm-relative wind vectors and wavenumber-1 component of the relative vorticity (colored, 10^{-5} s^{-1}) at (a) 24, (b) 48, (c) 72, (d) 96, (e) 120, and (f) 144 h. The plotting domain size is 2160 km × 2160 km. The dashed circles denote the radial distance every 300 km.

region is advected anticyclonically and outward by the symmetric components of the upper-level tangential flow and radial outflow, which causes the upper-level vorticity field to exhibit spiral patterns during the first 96 h (Figs. 5e,g,h). Different from the $HADV_1$ and $HADV_s$ terms, the nonlinear term $HADV_n$ induces a vorticity tendency opposite to the sign of the vorticity tendency in the south-southwest (north northeast) quadrant of the annulus with radii from 600 to 900 km (Fig. 5f) and therefore is unfavorable for the development of spiral vorticity bands in that region during the first 96 h.

From Fig. 6, it can be seen that the cyclonic rotation of the upper-level wavenumber-1 vorticity field in the period from 96 to 144 h is mainly induced by the β effect and the horizontal vorticity advection (Figs. 6a–c). The $HADV_1$ term produces the positive (negative) vorticity tendency on the west (east) side of the TC center (Fig. 6d). Meanwhile, the $HADV_s$ term contributes to the increase of the positive (negative) vorticity in the area extending from the southwest to southeast (northeast to northwest) side of the TC via the outward advection of the positive (negative) vorticity produced by the BETA and $HADV_1$ terms by the radial outflow (Figs. 6a,d,e,h). Except for the radial expansion, the pattern of the vorticity tendency induced by $HADV_n$ in the period from 96 to 144 h is not much different from that in the first 96 h (Figs. 5f and 6f).[1] However, the sign of the $HADV_n$ term is consistent with the sign of the vorticity tendency on the south and north side of area with a radius larger than 600 km (Fig. 6f). Therefore, the nonlinear interactions also make a contribution to the cyclonic rotation of the spiral vorticity bands in the period from 96 to 144 h.

Based on the above description, the evolution of the β shear can be divided into two stages. First, along with the

[1] Calculations indicate that the $HADV_n$ term is mainly induced by the interaction between the wavenumber-1 and -2 components. Because of the outward propagation of the wavenumber-2 component of vorticity, the area with positive (negative) $HADV_n$ located in the south (north) of the TC outer region experiences outward expansion.

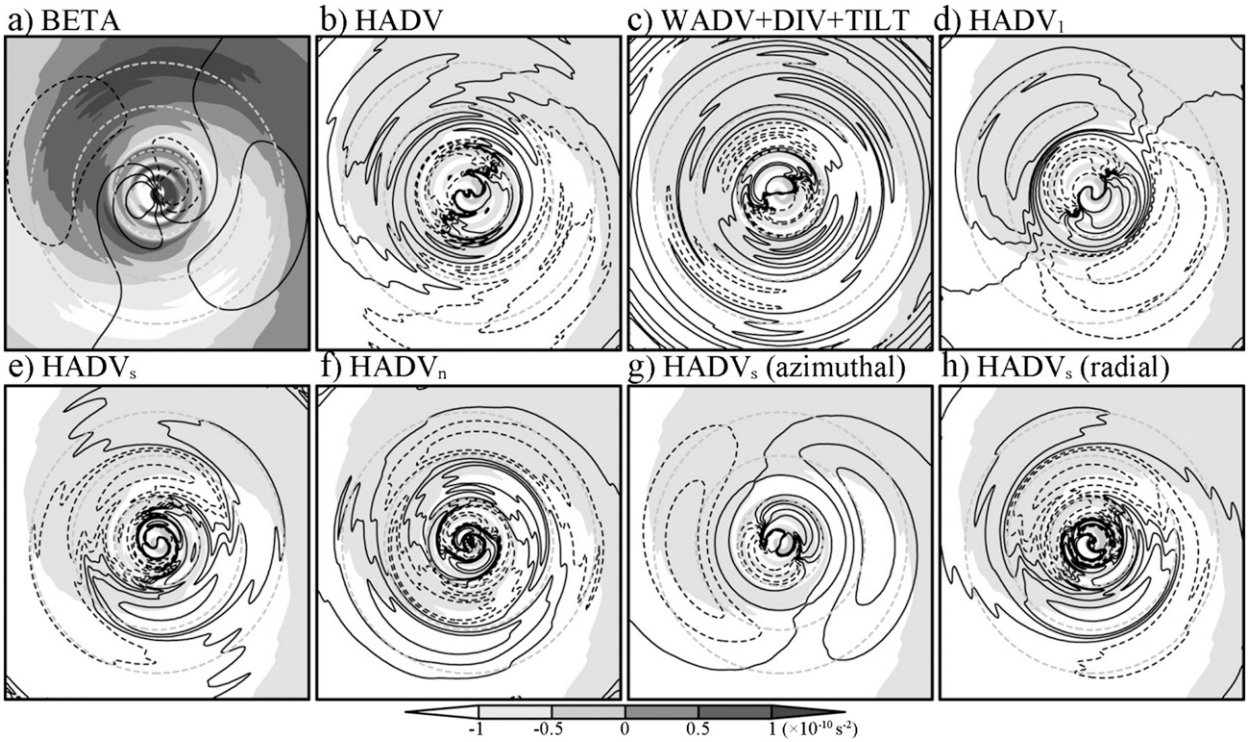

FIG. 5. The 0–96-h averaged tendency (10^{-10} s^{-2}) of the wavenumber-1 component of relative vorticity induced by (a) $-\beta\overline{v}$ (BETA), (b) horizontal advection, (c) vertical advection, stretching and tilting, (d) horizontal advection of the symmetric vorticity by the wavenumber-1 flow ($HADV_1$), (e) horizontal advection of the wavenumber-1 vorticity by the symmetric flow ($HADV_s$), (f) horizontal advection resulting from nonlinear interaction among asymmetric perturbations ($HADV_n$), and (g),(h) horizontal advection of the wavenumber-1 vorticity by the symmetric tangential and radial flows at $z = 12$ km in EXP-β. The contours are of the values of $(-30, -10, -5, -2, -1, 0, 1, 2, 5, 10, 30) \times 10^{-10}$ s^{-2} and negative is dashed. The time tendency of vorticity averaged in the period from 0 to 96 h is depicted by the shading in (a). The gray and white areas in (b)–(h) denote that the wavenumber-1 component of relative vorticity at 96 h is larger and smaller than that at 0 h, respectively. The gray dashed circles denote the radial distance every 300 km.

continuous increase (decrease) of the upper-level vorticity in the north-northeast (south southwest) of the TC outer region induced by the interactions between the symmetric and asymmetric components of the TC flow, northwesterly flow gradually develops and becomes dominant in the upper-level TC flow. As a result, the β shear is established and reaches a peak value of ~8.2 m s^{-1}. Second, the outward advection of the positive (negative) vorticity arising from the BETA and $HADV_1$ terms, and the horizontal advection associated with nonlinear interactions becomes strong enough to reverse the vorticity tendency established in the first stage and leads to an increase (decrease) of the upper-level vorticity in the southwest (northeast) quadrant of the TC outskirts. Hence, the northwesterly flow is weakened and gradually replaced by weak south-southwesterly flow in the upper levels. Consequently, the β shear decreases considerably.

5. Impact of β shear on TC convective structure

In EXP-β, the vertical wind shear is builtup gradually under the influence of the β effect and reaches a moderate strength (i.e., ~8.2 m s^{-1}), which may be taken as a prototype to investigate the impact of moderate shear on TCs. In this section, the effect of the β shear on TC convection will be examined to understand the differences between the convective activity simulated in EXP-*f* and EXP-β as shown in Figs. 2a–d.

a. Evolution of TC convection with and without β shear

Figure 7 shows 1-h mean vertical velocity at $z = 3$ km in the evolution of the TCs in EXP-*f* and EXP-β. Although there are some incoherent asymmetric signals, the vertical velocity field exhibits a nearly axisymmetric structure in the eyewall area in EXP-*f*, while its counterpart in EXP-β presents distinct asymmetries. At ~60 h when the β shear is well established (~4.5 m s^{-1}, Fig. 3) and becomes large enough to affect the vertical motion pattern of a TC, the strong ascent in the eyewall concentrates in the south-southeast side of the TC center (Fig. 7b). From 60 to 88 h, the updraft in the eyewall of the TC in EXP-β enhances along with the intensification of the TC, even though the β

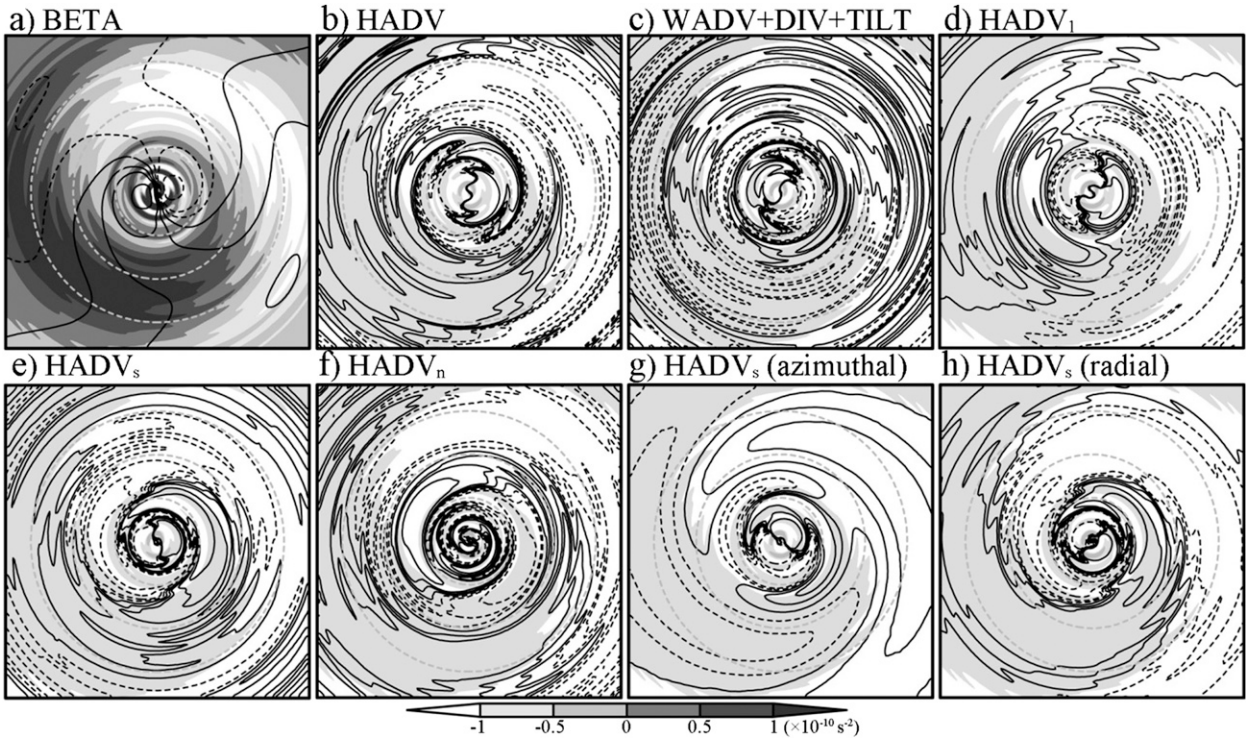

FIG. 6. As in Fig. 5, but the average period is from $t = 96$ to 144 h. (a) The shading depicts the time tendency of vorticity averaged in the period from 96 to 144 h and (b)–(h) the gray and white areas denote that the wavenumber-1 component of relative vorticity at 144 h is larger and smaller than that at 96 h, respectively.

shear gradually strengthens to its peak amplitude of ~8.2 m s^{-1}. In the meantime, the strongest ascent rotates cyclonically from the south to northeast side of the TC center (Fig. 7d). After 88 h, the β shear starts to decrease gradually (Fig. 3). Corresponding to a nearly fixed shear direction, the strong upward motion is mainly locked in the east-northeast quadrant of the eyewall (Figs. 7f,h,j,l). The asymmetric eyewall simulated in EXP-β is in agreement with earlier studies of the TC developed on a β plane (e.g., Bender 1997; Ritchie and Frank 2007) and can be explained by the effect of vertical wind shear on the TC (e.g., Jones 1995).

In addition to introducing the asymmetries in the eyewall, the β shear contributes to the occurrence of stratiform region outside of the eyewall in EXP-β. Figure 8 displays the radial–height distribution of reflectivity, wind, PV, and divergence in a vertical cross section directed from the TC center to the southeast in EXP-f and EXP-β at $t = 88$ h. Consistent with the distinct vertical wind shear, the radial outflow in the mid- to upper troposphere is stronger in EXP-β than that in EXP-f (Figs. 8a,c). As a result, the downwind advection of the ice particles generated within the eyewall updrafts is facilitated, which is favorable for the formation of a stratiform region at a relative far distance away from the eyewall in EXP-β (Houze 1993). From Figs. 8c,d near the radius of ~120 km, it can be seen that the kinematic structure of the model TC in EXP-β presents commonly observed features in stratiform regions that are loosely referred to as stratiform processes: a bright band located at an altitude of ~5 km, with mesoscale downdrafts below and updrafts above; convergence and positive PV are distinct in the midtroposphere and divergence occurs in the upper and low levels (e.g., Mapes and Houze 1995). In contrast, the above-mentioned features are not obvious in the TC simulated in EXP-f with similar range of radii (Figs. 8a,b).

To illustrate the evolution of the stratiform features under the effect of β shear, time–radius diagrams for the area of the stratiform region,[2] the filamentation time scale at $z = 5$ km, the azimuthal-mean equivalent potential temperature (Θ_e), and the vertical velocity at $z = 2$ km in both experiments are displayed in Fig. 9. In the

[2] The area of the stratiform region is evaluated by the number of points covered by stratiform cloud in the storm-centered circles following Rogers et al. (2007). Since the typical stratiform process is usually associated with low-level downdrafts, one more criterion is applied to the candidate stratiform regions identified from the method proposed by Rogers et al. (2007). That is whether the running mean of vertical motion anywhere within a 5-km distance of the location being considered is smaller than 0 m s^{-1}. If yes, then the location will be identified as stratiform region.

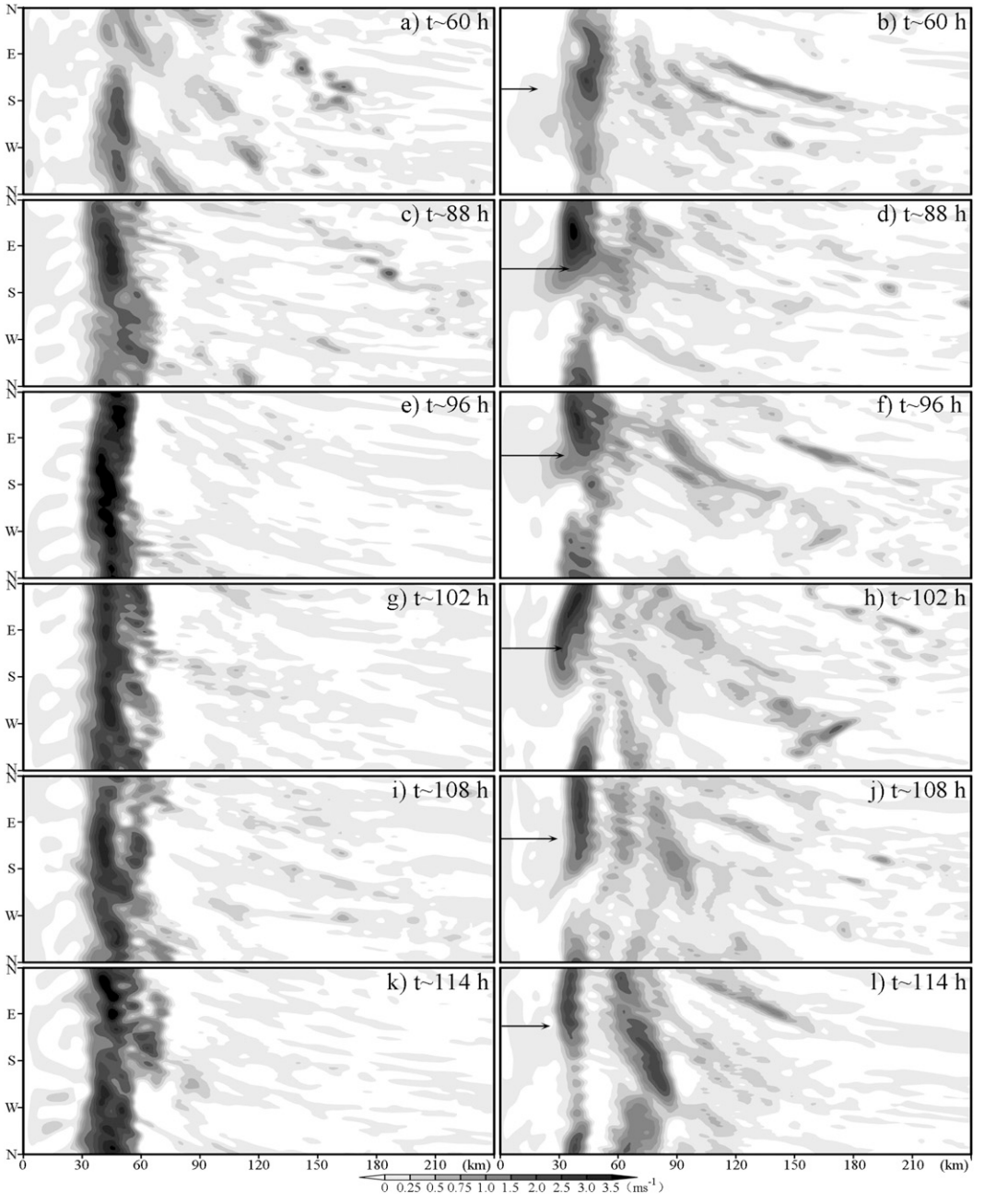

FIG. 7. Plan view of the 1-h mean vertical velocity at $z = 3$ km in the cylindrical coordinate obtained in (left) EXP-*f* and (right) EXP-β. Arrows in (right) denote the 1-h mean vertical wind shear marked in the direction the shear is pointing toward.

first 66 h (Figs. 9a,e), the stratiform precipitation occurs outside of the radius of 60 km and exhibits periodic outward propagation in both experiments. However, as the β shear increases, considerable stratiform clouds develop in the area outside the radius of 100 km in EXP-β after 66 h instead of only concentrating near the eyewall as that in EXP-*f*. After 88 h (Fig. 9e), when the β shear starts to decrease gradually, the stratiform region increases in coverage in the 90–180-km annulus in EXP-β, reminiscent of the axisymmetrizing process suggested by Wang (2006).

Because of the active stratiform clouds, distinct midlevel PV production occurs, and as a result, the midlevel PV is larger at radii larger than 100 km in EXP-β than that in EXP-*f* after 66 h (Figs. 9b,f). In addition to providing a supply of PV to the low-level flow via downward flux as suggested by Wang (2006) and May and Holland

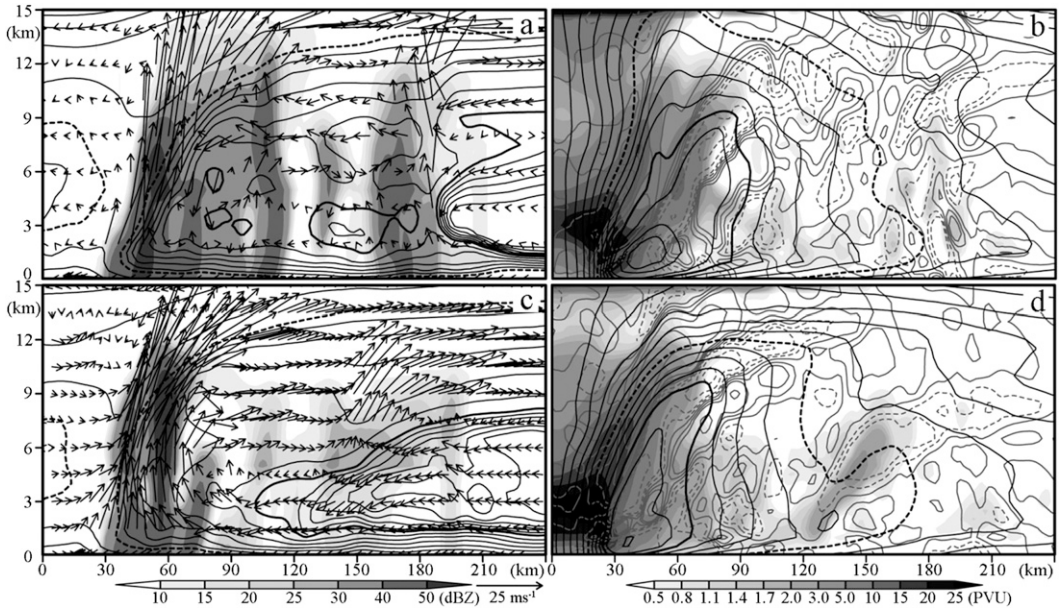

FIG. 8. (a) Height–radial distribution of the model-derived reflectivity (shaded), Θ_e (black contours), and wind vectors in the vertical cross section directed from the TC center to the southeast at 88 h in EXP-*f*. (b) As in (a), but for the potential vorticity (shaded), horizontal divergence (gray contours with negative dashed), and tangential wind (black contours with the interval of 5 m s^{-1}). (c),(d) As in (a),(b), but for EXP-β. The black thick solid and dashed contours in (a) and (c) denote the values of 343 and 355 K, respectively. The intervals of Θ_e contours are 1, 2, and 5 K respectively for values smaller than 343 K, smaller than 355 K but larger than 343 K, and larger than 355 K. The black thick solid and dashed contours in (b) and (d) denote the values of 30 and 50 m s^{-1}, respectively. In the wind vector field in (a) and (c), the vertical velocity has been 15 times amplified.

(1999), the midlevel PV can affect TC convection by modifying the filamentation time scale (τ_{fil}) defined as $[-(\overline{v}_t/r)(\partial\overline{v}_t/\partial r)]^{-1/2}$ by Terwey and Montgomery (2008) with $\overline{v}_t$ denoting the azimuthal-mean tangential velocity. From Figs. 8b,d we can see that, because of the distinct midlevel PV anomaly, the tangential wind and its radial gradient on the inner side of the midlevel PV maximum is weaker in EXP-β than EXP-*f*. Accordingly, the filamentation time scale outside of the radius of ~80 km is slightly longer in EXP-β than EXP-*f* after ~72 h (Figs. 9b,f). This indicates that the area beyond the radius of 80 km is a more convection-friendly region in EXP-β because the straining process there is relatively weak (Rozoff et al. 2006; Wang 2008a).

Similar to the midlevel PV, the low-level Θ_e also presents different features between EXP-*f* and EXP-β under the effect of stratiform processes (Figs. 9c,g). In EXP-*f* (Fig. 9c), the low-level Θ_e outside of the eyewall increases as the TC develops and the frontlike zone between the TC's warm and moist air and the environment moves outward gradually. However, owing to the evaporative cooling associated with the stratiform precipitation, the increase of the low-level Θ_e is considerably weaker outside the radius of 120 km in EXP-β (Fig. 9g). Consequently, the outward movement of the frontlike zone beyond the eyewall is almost terminated after ~84 h when the frontlike zone moves to the radius of ~120 km in EXP-β.

From Fig. 9g, we can see that the frontlike zone is accompanied by distinct positive horizontal vorticity in the tangential direction ($\eta = \partial u/\partial z - \partial w/\partial r$). To evaluate the contribution of the thermal contrast across the frontlike zone to the maintenance of the positive η, the budget of η is conducted following Ziegler et al. (1995) and Brandes (1984) as

$$\frac{\partial \eta}{\partial t} = -u\frac{\partial \eta}{\partial r} - w\frac{\partial \eta}{\partial z} + \left(f_c + \frac{2v}{r} + \frac{u}{r}\right)\frac{\partial v}{\partial z} - \eta\left(\frac{\partial u}{\partial r} + \frac{u}{r} + \frac{\partial w}{\partial z}\right) - c_p\frac{\partial \theta_{v0}}{\partial z}\frac{\partial \pi'}{\partial r} - g\frac{\partial}{\partial r}\left(\frac{\theta'}{\theta_0} + 0.61q_v'\right) + \left(\frac{\partial F_r}{\partial z} - \frac{\partial F_z}{\partial r}\right), \quad (4)$$

where r and z are the radius and height, respectively; c_p is the specific heat at constant pressure; θ_0 and θ_{v0} are the base-state potential and virtual potential temperatures, respectively; π' is the perturbation Exner function (or simply perturbation pressure); g is the acceleration of gravity; θ' is the perturbation potential temperature; q_v' is the perturbation vapor mixing ratio; and F represents

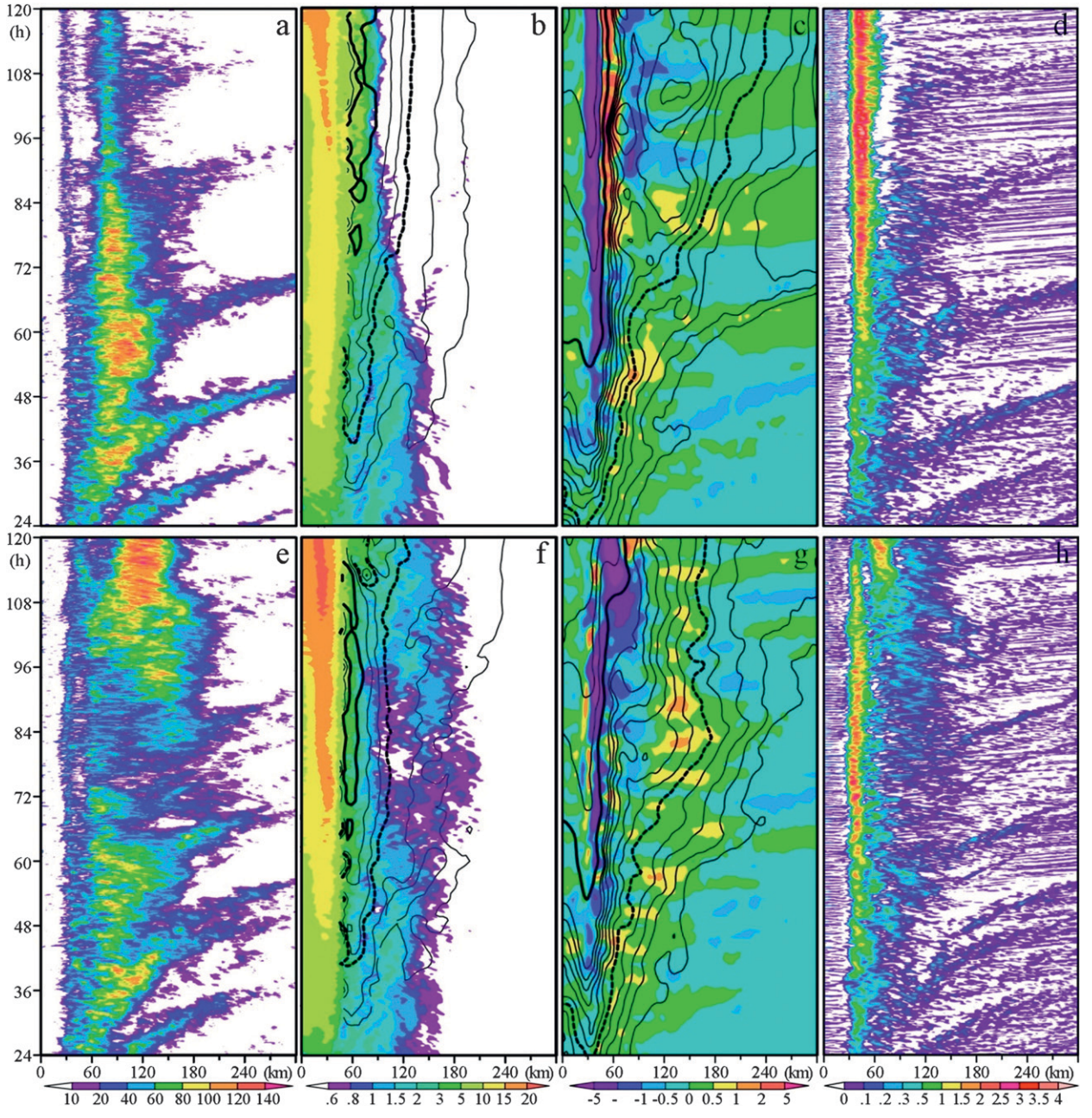

FIG. 9. (a) Time evolution of the area of stratiform cloud in the storm-centered circles in EXP-*f*. (b) The azimuthal-mean potential vorticity averaged from $z = 4.5$ to 6 km [shading; units: potential vorticity unit (PVU), 1 PVU $= 10^{-6}$ K m^2 kg^{-1} s^{-1}], filamentation time scales at $z = 3$ km (contours with the intervals of 10 and 40 min for the values smaller and larger than 60 min). (c) As in (b), but for Θ_e (contours with intervals of 1 and 4 K for values smaller and larger than 350 K, respectively) and horizontal vorticity (η, shading, units: 10^{-3} s^{-1}) at $z = 3$ km. (d) As in (a), but for the vertical velocity at $z = 3$ km (units: m s^{-1}). (e)–(h) As in (a)–(d), but for EXP-β. The thick solid and dotted contours denote the filamentation time scales of 30 and 60 min in (b) and (f) and the Θ_e of 350 and 340 K in (c) and (g), respectively. The area of stratiform cloud in (a) is evaluated by the number of points covered by stratiform cloud in the storm-centered circles.

the subgrid-scale turbulence force. All perturbations are deviations from the base state, which is itself a function of height. The terms in the right-hand side of Eq. (4) are the advection, Coriolis, stretching, pressure solenoid, thermal, and turbulent terms, respectively, the contributions of which to the tendency of η in EXP-β are illustrated in Fig. 10. It is clear that the thermal contrast across the frontlike zone makes an essential contribution to the maintenance of the positive η beyond the eyewall (Fig. 10c). This implies that the frontlike feature is beneficial to the

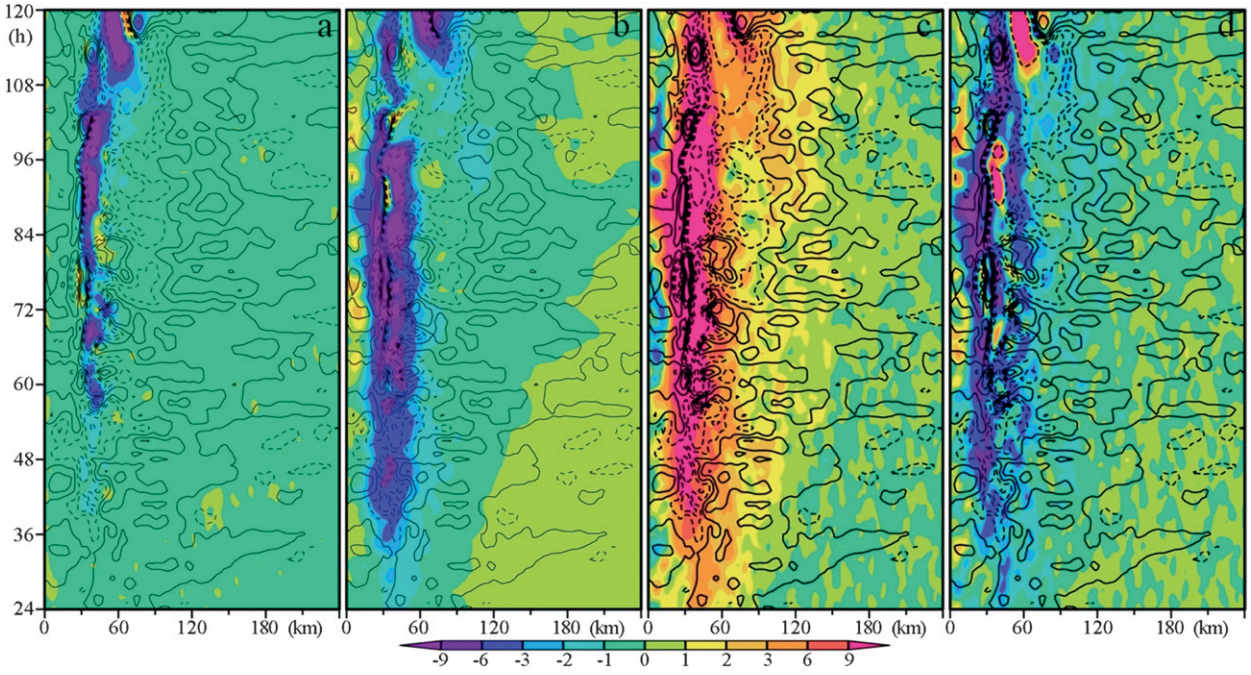

FIG. 10. Time evolutions of the azimuthal-mean tendency (units: 10^{-6} s^{-1}) of horizontal vorticity (η) induced by (a) the advection, stretching, and pressure solenoid; (b) Coriolis; (c) thermal; and (d) turbulent terms in Eq. (4) at $z = 3$ km in EXP-β. The contours denote the horizontal vorticity at $z = 3$ km with the values of $(-5, -2, -1, -0.5, 0, 0.5, 1, 2, 5) \times 10^{-3}$ s^{-1} and negative is dashed.

convective activity outside of the eyewall via providing necessary lifting in the upward branch of the direct thermal circulation associated with the positive η. It is worthwhile mentioning that, although the vorticity tendency resulting from the radial gradient of potential temperature is much greater than that related to the radial gradient of specific humidity in Eq. (4), the latter does make a positive contribution to the positive tendency of η in the frontlike zone in EXP-β. Therefore, the radial variation of Θ_e is adopted to denote the frontlike zone in this study.

The relatively long filamentation time scale and the significant thermal contrast induced by the active stratiform processes, together with the moderate convective available potential energy (CAPE) and weak convection inhibition (CIN; Fig. 11) make the inner edge of the frontlike zone a convective-friendly region. As a result, distinct upward motion occurs right inside of the radius of 120 km after ~88 h in EXP-β (Figs. 7d,f,h,j,l and 9h). Although there is convective potential and the filamentation time scale is longer than 30 min outside of the radius of 80 km, the convection is rather weak and sporadic in the area beyond the eyewall in EXP-*f* (Figs. 7c,e,g,i,k and 9d). This implies that the nearly stationary frontlike zone associated with the stratiform precipitation plays an important role in the convective activity outside of the eyewall in EXP-β. In addition to maintaining the stationary frontlike zone, the evaporative cooling below the stratiform cloud also favors convective bursts by decreasing the low-level stability and reducing the value of boundary layer Θ_e that is needed for convection to occur as suggested by Bister and Emanuel (1997).

b. *Development of a convective ring outside of the eyewall in EXP-β*

Recent studies on concentric eyewalls of TC indicates that a well-defined low-level β skirt and sufficient τ_{fil} are favorable for the formation of a well-organized convective band outside the eyewall via maintenance of long-lasting deep convection and upscale transfer of energy

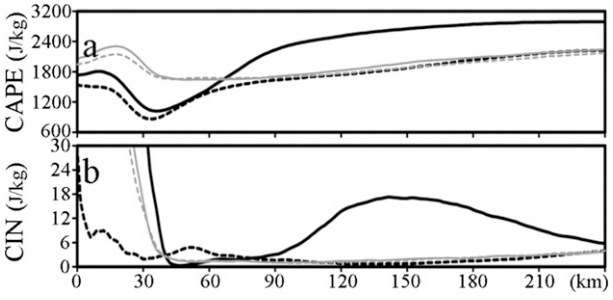

FIG. 11. Radial distribution of the mean symmetric (a) surface-based CAPE, and (b) the amount of energy required to overcome the negative buoyant energy the environment exerts on an air parcel at $z = 1.5$ km in the period from $t = 1$ to 72 h (gray) and $t = 73$ to 120 h (black) in EXP-*f* (solid) and EXP-β (dash).

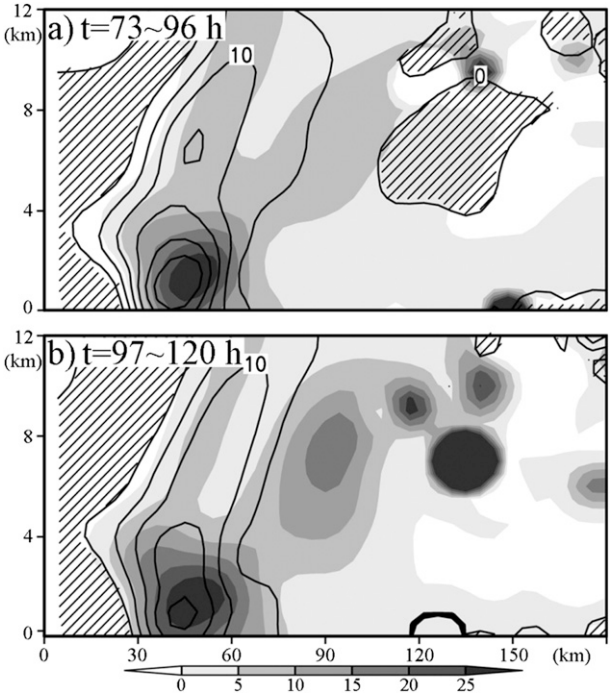

FIG. 12. (a) Vertical cross section of the mean effective β (units: 10^{-8} m^{-1} s^{-1}) averaged from $t = 73$ to 96 h in EXP-f (shaded) and EXP-β (contours). (b) As in (a), but for the period from $t = 97$ to 120 h. The regions with negative mean effective β in EXP-f and EXP-β are denoted by the white and hatched areas, respectively.

from convection-scale motion (e.g., Terwey and Montgomery 2008; Qiu and Tan 2010). Figure 12 presents the vertical cross section of the 24-h and azimuthal mean effective β calculated in both experiments. Following Terwey and Montgomery (2008), the effective β is defined as $(-\partial\overline{q}/\partial r)(\overline{\xi}/\overline{q})$ with $\overline{q}$, and $\overline{\xi} = f_c + 2\overline{v}_t/r$ denoting the azimuthal mean PV and modified Coriolis parameter. From the contours shown in Fig. 12 we can see that the low-level effective β averaged in the period from 73 to 96 h and 97 to 120 h is strictly positive out to the radius of ~120 km in EXP-β. Therefore, there is a β skirt outside of the eyewall to constrain the asymmetric flow and facilitate the transfer of perturbation vorticity and kinetic energy from sporadic deep convection to the azimuthal mean flow as predicted by quasi-linear axisymmetrization dynamics (Terwey and Montgomery 2008). Besides the β skirt, Fig. 9f shows that the filamentation time scale is much longer than 30 min outside the radius of 60 km in EXP-β, which is sufficient for the growth of convection on the inner edge of the frontlike zone instead of it being disrupted by the straining process (Rozoff et al. 2006; Wang 2008a). Consistent with the β-skirt axisymmetrization (BSA) formation hypothesis for the development of the secondary eyewall suggested by Terwey and Montgomery (2008), the convection outside of the eyewll is organized to form a well-defined convective ring in EXP-β (Figs. 7l and 9h), as also found in Wang (2006).

Figure 13 shows the development of the convective ring beyond the eyewall from a radius–height prospective. At ~84 h (Fig. 13a), the frontlike zone situates right outside the radius of 120 km. About 6 h later (Fig. 13b), the inner edge of the frontlike zone moves to the radius of ~105 km and the thermal contrast across it considerably increases. This is mainly caused by active convection on the inner edge of the frontlike zone, which releases diabatic heating to increase Θ_e on the inner edge of the frontlike zone. The inward movement of the frontlike zone is similar to the contraction of the TC wind maximum described by Shapiro and Willoughby (1982) and Willoughby et al. (1982); that is, the diabatic heating near the eyewall causes the rapid increase of the tangential wind just inside the radius of maximum wind and leads the TC wind maximum moving inward. As a result of the strengthening low-level Θ_e gradient and the inward movement of the frontlike zone, enhanced convection appears right outside the radius of ~90 km at 97 h (Fig. 13c). In addition to the release of diabatic heating, convection can strengthen the low-level Θ_e gradient via facilitating the outward transfer of the high low-level Θ_e from the eyewall region. From Fig. 13a we can see that there is shallow outward flow immediately above the inflow layer under the eyewall, which is induced by the supergradient winds near the top of the inflow boundary layer (Kepert 2001; Kepert and Wang 2001). At ~104 h (Fig. 13d), the outflow expands outward to the radius of ~90 km. This may be induced by the low-level convergence accompanying the convection on the inner edge of the frontlike zone (Fig. 13d). As a result of the outward transfer of the high low-level Θ_e from the eyewall region, the low-level Θ_e gradient is enhanced considerably at around $r = 90$ km. Meanwhile, the outward transfer of warm and moist air from the eyewall caused by the outflow right above the inflow layer leads to a convectively unstable environment in the lower troposphere, which together with the increasing radial gradient of low-level Θ_e (and negligible CIN), contributes to the development of convection at the inner edge of the frontlike zone (Fig. 13d). This convection finally merges with the inner convection near the radius of 60 km resulting in vigorous convection in the annulus with radii between 60 and 90 km (Fig. 13e).

The evolution of the vertical velocity at $z = 3$ km shown in Fig. 7 illustrates the development of the well-organized convective band outside of the eyewall in the horizontal view.

From Fig. 7, it can be seen that, right outside of the eyewall ($r < 70$ km), there are inner convective bands developing in both experiments, which may originate

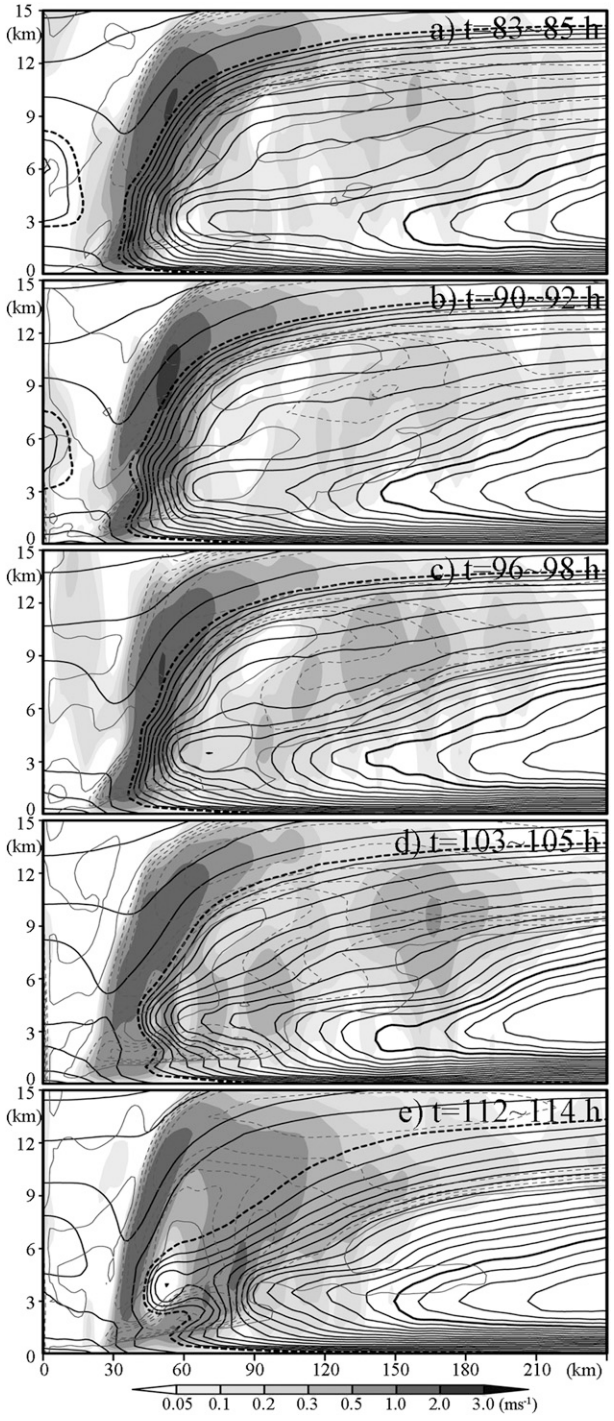

FIG. 13. Vertical cross section of the 3-h-azimuthal-mean vertical velocity (shaded), Θ_e (black contours), and radial outward velocity (gray contours) in EXP-β. The black thick solid and dashed contours denote the values of 342 and 355 K, respectively. The intervals of Θ_e contours are 1 and 5 K, respectively, for values smaller and larger than 355 K. The radial outward velocity is contoured at 0 (solid contour), 1, 2, 3, 4, 5, 10, 20, 30, and 40 m s^{-1}.

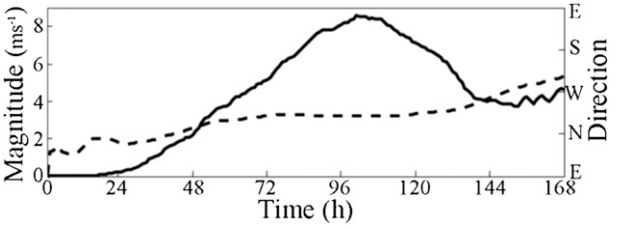

FIG. 14. Time evolutions of the magnitude (thick line) and direction (dashed line) of the vertical wind shear between $z = 1.5$ and 12 km in the sensitivity experiment similar to EXP-β, except that the microphysics associated with solid ice is turned off.

from the asymmetric eyewall (Wang 2008b). In a father distance from the eyewall, the initially active convection dissipates gradually after 88 h and a moat appears between the eyewall and the weak and sporadic convection occurred beyond the radius of ~85 km in EXP-*f* (left column of Fig. 7). However, because of the distinct stratiform region induced by the β shear, the convection outside of the radius of 70 km remains strong and active after $t = 88$ h in EXP-β, which becomes more organized in the azimuthal direction and eventually merges with the inner convective bands. Eventually, a quasi-axisymmetric convective band forms beyond the primary eyewall similar to that in Wang (2006) (Figs. 7j,l).

c. *The importance of stratiform processes*

From Figs. 9b, 11, and 12, it can be found that a substantial overlap between the β skirt and an area of strong convective potential (i.e., large filamentation time scale, sufficient CAPE, and low CIN) occurs in the region beyond $r = 60$ km in EXP-*f*, which is consistent with the BSA formation hypothesis suggested by Terwey and Montgomery (2008). However, there are no well-organized convective bands outside the eyewall in EXP-*f* as there are in EXP-β, which indicates that the asymmetric forcing induced by the β effect (i.e., β shear) plays an essential role in the development of the well-organized convective ring outside of the eyewall. (the dynamics of the secondary eyewall formation in EXP-beta is the focus of a companion study Rozoff et al. 2012).

To further understand how the β shear affects the convective bands outside of the eyewall, a sensitivity experiment similar to EXP-β is conducted except that the processes associated with solid ice are terminated. Figure 14 shows the β shear developed in this additional sensitivity experiment. It is obvious that, because of the β effect, the β shear develops and evolves in a similar way as that in EXP-β. However, the upward motion in the outer convective bands (except for the inner convective bands immediately outside of the eyewall) is very weak as compared to that in EXP-β and no well-organized convective ring developed outside of the eyewall (Fig. 15).

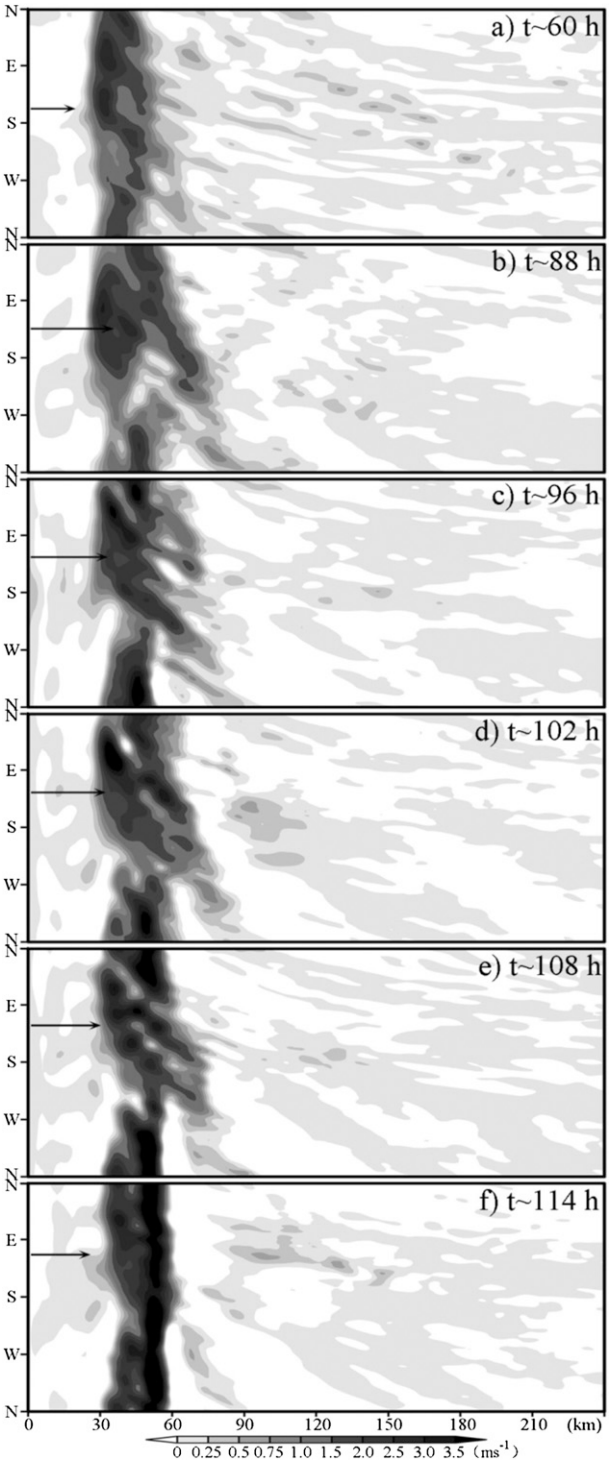

FIG. 15. Plan view of the 1-h mean vertical velocity at $z = 3$ km in the cylindrical coordinate obtained in the sensitivity experiment similar to EXP-β, except that the microphysics associate with solid ice is turned off. Arrows denote the 1-h mean vertical wind shear marked in the direction the shear is pointing toward.

The sensitivity experiment together with EXP-*f* and EXP-β indicates that the stratiform processes may be an important contributor to the development of the convective ring outside of the eyewall as suggested by Wang (2006) and Zhou and Wang (2011).

6. Conceptual model for the evolution and impacts of β shear

Based on the above discussions of the β shear and convective structure in EXP-β, the structural evolution of a TC developed in an environment with variable Coriolis parameter could be summarized into three consecutive stages: 1) buildup of β shear and asymmetric inner rainbands; 2) increase and peak in β shear, development of extensive stratiform region, and initiation of outer convective rainbands; and 3) reduction in β shear and formation of the quasi-axisymmetric convective band.

a. Stage 1: Buildup of β shear and asymmetric inner rainbands

As a TC develops in the environment with variable *f*, the advection of the planetary vorticity by the TC circulation induces asymmetries at both the low and upper levels. The advection of the symmetric (asymmetric) vorticity by the asymmetric (symmetric) flow results in the development of a negative (positive) vorticity perturbation in the southwest (northeast) quadrant of the TC in the upper levels, which is opposite to that in the low levels (Figs. 16a,b, left). As a result, the vertical wind shear is established and intensifies gradually as the TC intensifies (Fig. 16c, left).[3] Under the effect of β shear, the deep convection in the eyewall mainly occurs in the downshear to downshear-left region and the updraft exhibits distinct outward spreading from the eyewall in the mid- to upper levels (Figs. 16c,d, left).

b. Stage 2: Increase and peak in β shear, development of extensive stratiform region, and initiation of outer convective rainbands

Along with the TC intensification, the asymmetric perturbations in both the low and upper levels are continuously enhanced, leading to the increase of the β shear to a peak value of ~8.2 m s^{-1} (Figs. 16a–c, middle). Meanwhile, a stratiform region develops outside of the eyewall (Figs. 16c,d, middle), which plays an important role in the initiation and organization of convection by preconditioning the dynamic and thermodynamic environment

[3] To illustrate the evolution of the flow patterns properly, the wind displayed in Fig. 16 is the total wind in contrast to the storm-relative wind shown in Fig. 2.

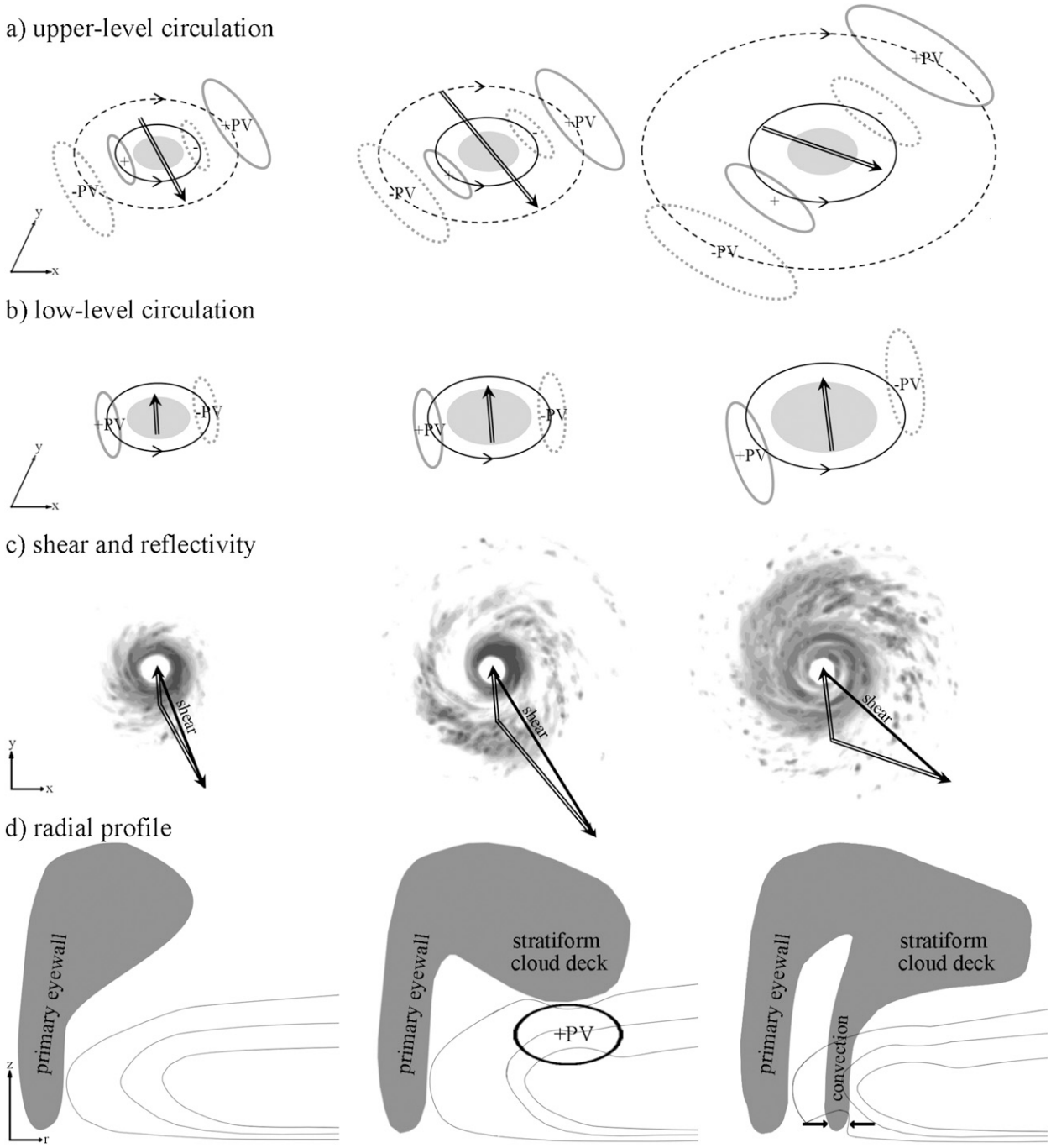

FIG. 16. (a) Schematic diagram for the evolution of the upper-level circulation in TCs developed in the variable-f environment. Gray shading denotes the symmetric PV with values larger than zero. Black solid and dashed ellipses indicate the symmetric cyclonic and anticyclonic flows, respectively. Gray solid and dashed ellipses represent the positive and negative PV anomalies, respectively. (b) As in (a), but for the low-level circulation. (c) As in (a), but for the area-mean storm-relative winds at the lower and upper levels (hollow arrows), β shear (solid arrows), and 5-km reflectivity (shading). (d) As in (c), but for the evolution of the convection (shading) and low- to midlevel Θ_e (contour) in the vertical cross section. Black ellipses and arrows denote the midlevel positive PV anomalies and low-level flows associated with the outer convection, respectively.

near the stratiform region. On one hand, the substantial concentration of the positive PV in the midlevels (Fig. 16d, middle) resulting from the mid- to upper-level condensational heating and low-level cooling associated with stratiform processes tends to weaken the radial gradient of tangential wind nearby, which is beneficial to the growth of convection through prolonging the filamentation time scale. On the other hand, the evaporative

cooling below the stratiform region slows down the increase of the low-level Θ_e, which favors more convective bursts at least in two ways. First, it suppresses the radial outward expansion of the high Θ_e air from the TC inner core and then sharpens the Θ_e gradient near the stratiform region. Such a process is beneficial to convective bursts by providing necessary lifting. Second, it decreases the low-level stability (Fig. 16d, middle) and reduces the value of boundary layer Θ_e that is needed for convection to occur (Bister and Emanuel 1997). Consequently, convection is active near the stratiform region (Fig. 16c, middle), which further increases the Θ_e gradient nearby via latent heating and advection of high Θ_e air from the eyewall.

c. *Stage 3: Reduction in β shear and formation of the quasi-axisymmetric convective band*

The wavenumber-1 component of the upper-level vorticity changes greatly between stages 2 and 3 (Figs. 16a,b, right). The negative (positive) vorticity anomaly located in the southwest (northeast) quadrant of the TC moves outward gradually (Fig. 16a, right) and its impact on the TC circulation is diminishing. In the meantime, the outward advection of the positive (negative) vorticity produced to the southwest (northeast) of the TC central area by the intensified radial outflow leads to the enhancement of the positive (negative) vorticity to the southwest (northeast) of the TC (Fig. 16a, right). As a result, the northwesterly winds over the TC, being distinct in stage 2, are reduced substantially while the area-mean wind shifts cyclonically (Fig. 16a, right). Consequently, the β shear weakens considerably (Fig. 16c, right). The weakening of the β shear and a substantial overlap between the β skirt and an area of large filamentation time scale facilitate the axisymmetrization of the convective bands outside of the primary eyewall into a secondary-eyewall-like convective band followed by the decay of the original eyewall (Fig. 16d, right).

7. Summary and discussion

The current study examines the β effect on the evolution of TCs through comparing cloud-resolving WRF simulations with constant versus variable Coriolis parameters. It is found that the TC simulated on a β plane is relatively weaker in intensity while larger in size and strength than that on an *f* plane. The meridional gradient of the planetary vorticity across the TC circulation is primarily responsible for the differences in storm intensity and size, while the effect of increasing *f* due to the movement of the TC to higher latitude is rather secondary.

As a result of the β effect, the β shear is established and then strengthened as the TC intensifies, which causes the convective structure of the TC developed on the β plane to exhibit a different pattern from that on the *f* plane. In addition to introducing distinct asymmetries in the eyewall with the strongest ascent concentrated on the downshear to downshear-left side, the β shear also plays an important role in the development of the active stratiform clouds in the TC outer region. The processes associated with the stratiform clouds are favorable for convective activity through producing substantial mid-level PV anomalies to prolong the filamentation time scale, and through sharpening the low-level Θ_e gradient to promote stronger convective bursts near the inner edge of the stratiform region. As a result, the convection is more active in the TC outer region in EXP-β than that in EXP-*f*. As the TC evolves, the outer convection is strengthened and well organized, and finally leads to the formation of a quasi-axisymmetric convective band in EXP-β. The development of the convective ring beyond the eyewall leads to a relatively weaker TC in intensity while larger in size than that on an *f* plane (Xu and Wang 2010a,b; Wang 2009; Hill and Lackmann 2009; Hack and Schubert 1986). The evolution of the TC structure simulated in the variable-*f* experiment can be summarized into a three-stage conceptual model: 1) establishment and development of the β shear and asymmetric rainbands; 2) increase and peak in the β shear, development of an extensive stratiform region, and initiation of outer convective rainbands; and 3) reduction in the β shear and formation of a quasi-symmetric convective band outside of the eyewall.

It is worth mentioning that, although the TC simulated in EXP-β exhibits a well-defined convective ring outside the eyewall with a secondary maximum of the azimuthal-mean tangential wind, the TC intensity in terms of the minimum sea level pressure and maximum 10-m azimuthal-mean tangential wind shows no clear weakening as the circular convective bands develop. Therefore, the well-organized convective ring outside of the eyewall simulated in EXP-β may not be taken as the representative secondary eyewall described by Willoughby et al. (1982) and many others in the literature. The recent work of Kuo et al. (2009) indicates that not all the TCs with concentric eyewalls weaken 24 h after formation of double eyewall.

Acknowledgments. The research was conducted during the first author's sabbatical visits at Texas A&M and Penn State University. The authors are grateful to Robert Rogers for providing us with the code on classification algorithm for eyewall, rainband, and stratiform regions and to Dave Nolan, Chris Rozoff, Bill Frank, Yuqing Wang, Yonghui Weng, and two anonymous reviewers for their constructive comments. This work was supported in part by Nature Science Foundation of China Grants 40921160382 and 41130964,

State Key Basic Program of China 2012CB417201, and by Office of Naval Research Grant N000140910526, NOAA HFIP Grant NA12NWS4680001, and National Science Foundation Grant AGS 0840651.

REFERENCES

Bender, M. A., 1997: The effect of relative flow on the asymmetric structure in the interior of hurricanes. *J. Atmos. Sci.,* **54,** 703–724.

Bister, M., and K. A. Emanuel, 1997: The genesis of Hurricane Guillermo: TEXMEX analyses and a modeling study. *Mon. Wea. Rev.,* **125,** 2662–2682.

Brandes, E. A., 1984: Relationships between radar-derived thermodynamic variables and tornadogenesis. *Mon. Wea. Rev.,* **112,** 1033–1052.

Carr, L. E., and R. T. Williams, 1989: Barotropic vortex stability to perturbations from axisymmetry. *J. Atmos. Sci.,* **46,** 3177–3191.

Chan, J. C.-L., and R. T. Williams, 1987: Analytical and numerical studies of the beta-effect in tropical cyclone motion. Part I: Zero mean flow. *J. Atmos. Sci.,* **44,** 1257–1265.

DeMaria, M., and W. Schubert, 1984: Experiments with a spectral tropical cyclone model. *J. Atmos. Sci.,* **41,** 901–924.

Fiorino, M., and R. L. Elsberry, 1989: Some aspects of vortex structure related to tropical cyclone motion. *J. Atmos. Sci.,* **46,** 975–990.

Hack, J. J., and W. H. Schubert, 1986: Nonlinear response of atmospheric vortices to heating by organized cumulus convection. *J. Atmos. Sci.,* **43,** 1559–1573.

Hill, K. A., and G. M. Lackmann, 2009: Influence of environmental humidity on tropical cyclone size. *Mon. Wea. Rev.,* **137,** 3294–3315.

Holland, G. J., 1983: Tropical cyclone motion: Environmental interaction plus a beta effect. *J. Atmos. Sci.,* **40,** 68–75.

——, and R. T. Merrill, 1984: On the dynamics of tropical cyclone structural changes. *Quart. J. Roy. Meteor. Soc.,* **110,** 723–745.

Hong, S.-Y., J. Dudhia, and S.-H. Chen, 2004: A revised approach to ice microphysical processes for the parameterization of clouds and precipitation. *Mon. Wea. Rev.,* **132,** 103–120.

Houze, R., 1993: *Cloud Dynamics*. Academic Press, 573 pp.

Jones, S. C., 1995: The evolution of vortices in vertical shear. I: Initially barotropic vortices. *Quart. J. Roy. Meteor. Soc.,* **121,** 821–851.

Jordan, C. L., 1958: Mean soundings for the West Indies area. *J. Meteor.,* **15,** 91–97.

Kepert, J. D., 2001: The dynamics of boundary layer jets within the tropical cyclone core. Part I: Linear theory. *J. Atmos. Sci.,* **58,** 2469–2484.

——, and Y. Wang, 2001: The dynamics of boundary layer jets within the tropical cyclone core. Part II: Nonlinear enhancement. *J. Atmos. Sci.,* **58,** 2485–2501.

Kuo, H.-C., C.-P. Chang, Y.-T. Yang, and H.-J. Jiang, 2009: Western North Pacific typhoons with concentric eyewalls. *Mon. Wea. Rev.,* **137,** 3758–3770.

Kwok, H. Y., and J. C. L. Chan, 2005: The influence of uniform flow on tropical cyclone intensity change. *J. Atmos. Sci.,* **62,** 3193–3212.

Liang, X., and J. C. L. Chan, 2005: The effects of the full Coriolis force on the structure and motion of a tropical cyclone. Part I: Effects due to vertical motion. *J. Atmos. Sci.,* **62,** 3825–3830.

Madala, R. V., and S. A. Piacsek, 1975: Numerical simulation of asymmetric hurricanes on a beta-plane with vertical shear. *Tellus,* **27,** 453–468.

Mapes, B. E., and R. A. Houze Jr., 1995: Diabatic divergence profiles in western Pacific mesoscale convective systems. *J. Atmos. Sci.,* **52,** 1807–1828.

May, P. T., and G. J. Holland, 1999: The role of potential vorticity generation in tropical cyclone rainbands. *J. Atmos. Sci.,* **56,** 1224–1228.

Merrill, R. T., 1984: A comparison of large and small tropical cyclones. *Mon. Wea. Rev.,* **112,** 1408–1418.

Montgomery, M. T., M. E. Nicholls, T. A. Cram, and A. B. Saunders, 2006: A vertical hot tower route to tropical cyclogenesis. *J. Atmos. Sci.,* **63,** 355–386.

Nguyen, S. V., R. K. Smith, and M. T. Montgomery, 2008: Tropical-cyclone intensification and predictability in three dimensions. *Quart. J. Roy. Meteor. Soc.,* **134,** 563–582.

Noh, Y., W.-G. Cheon, S.-Y. Hong, and S. Raasch, 2003: Improvement of the K-profile model for the planetary boundary layer based on large eddy simulation data. *Bound.-Layer Meteor.,* **107,** 401–427.

Nolan, D. S., 2007: What is the trigger for tropical cyclogenesis? *Aust. Meteor. Mag.,* **56,** 241–266.

Peng, M. S., B. F. Jeng, and R. T. Williams, 1999: A numerical study on tropical cyclone intensification. Part I: Beta effect and mean flow effect. *J. Atmos. Sci.,* **56,** 1404–1423.

Qiu, X., and Z.-M. Tan, 2010: The role of vortex–Rossby waves in hurricane secondary eyewall formation. *Mon. Wea. Rev.,* **138,** 2092–2109.

Reasor, P. D., M. T. Montgomery, and L. D. Grasso, 2004: A new look at the problem of tropical cyclones in vertical shear flow: Vortex resiliency. *J. Atmos. Sci.,* **61,** 3–22.

Ritchie, E. A., and W. M. Frank, 2007: Interactions between simulated tropical cyclones and an environment with a variable Coriolis parameter. *Mon. Wea. Rev.,* **135,** 1889–1905.

Rogers, R. F., M. L. Black, S. S. Chen, and R. A. Black, 2007: An evaluation of microphysics fields from mesoscale model simulations of tropical cyclones. *J. Atmos. Sci.,* **64,** 1811–1834.

Rotunno, R., and K. A. Emanuel, 1987: An air-sea interaction theory for tropical cyclones. Part II: Evolutionary study using a nonhydrostatic axisymmetric numerical model. *J. Atmos. Sci.,* **44,** 542–561.

Rozoff, C. M., W. H. Schubert, B. D. McNoldy, and J. P. Kossin, 2006: Rapid filamentation zones in intense tropical cyclones. *J. Atmos. Sci.,* **63,** 325–340.

——, D. S. Nolan, J. P. Kossin, F. Zhang, and J. Fang, 2012: The roles of an expanding wind field and inertial stability in tropical cyclone secondary eyewall formation. *J. Atmos. Sci.,* **69,** 2621–2643.

Shapiro, L. J., and H. E. Willoughby, 1982: The response of balanced hurricanes to local sources of heat and momentum. *J. Atmos. Sci.,* **39,** 378–394.

Skamarock, W. C., J. B. Klemp, J. Dudhia, D. O. Gill, D. M. Barker, W. Wang, and J. G. Powers, 2005: A description of the Advanced Research WRF Version 2. NCAR Tech. Note 468+STR, 88 pp.

Terwey, W. D., and M. T. Montgomery, 2008: Secondary eyewall formation in two idealized, full-physics modeled hurricanes. *J. Geophys. Res.,* **113,** D12112, doi:10.1029/2007JD008897.

Wang, Y., 2006: Concentric eyewall simulated in a fully compressible, nonhydrostatic, multiply nested, movable mesh tropical cyclone model (TCM4). Preprints, *27th Conf. on Hurricanes and Tropical Meteorology,* Monterey, CA, Amer. Meteor. Soc., 6B.6. [Available online at https://ams.confex.com/ams/27Hurricanes/techprogram/paper_107727.htm.]

——, 2008a: Rapid filamentation zone in a numerically simulated tropical cyclone. *J. Atmos. Sci.,* **65,** 1158–1181.

——, 2008b: Structure and formation of an annular hurricane simulated in a fully compressible, nonhydrostatic model—TCM4. *J. Atmos. Sci.,* **65,** 1505–1527.

——, 2009: How do outer spiral rainbands affect tropical cyclone structure and intensity? *J. Atmos. Sci.,* **66,** 1250–1273.

——, and G. J. Holland, 1996a: The beta drift of baroclinic vortices. Part I: Adiabatic vortices. *J. Atmos. Sci.,* **53,** 411–427.

——, and ——, 1996b: The beta drift of baroclinic vortices. Part II: Diabatic vortices. *J. Atmos. Sci.,* **53,** 3737–3756.

Willoughby, H. E., J. A. Clos, and M. G. Shoreibah, 1982: Concentric eye walls, secondary wind maxima, and the evolution of the hurricane vortex. *J. Atmos. Sci.,* **39,** 395–411.

——, F. D. Marks, and R. J. Feinberg, 1984: Stationary and moving convective bands in hurricanes. *J. Atmos. Sci.,* **41,** 3189–3211.

Wu, L., and S. A. Braun, 2004: Effects of environmentally induced asymmetries on hurricane intensity: A numerical study. *J. Atmos. Sci.,* **61,** 3065–3081.

Xu, J., and Y. Wang, 2010a: Sensitivity of tropical cyclone inner core size and intensity to the radial distribution of surface entropy flux. *J. Atmos. Sci.,* **67,** 1831–1852.

——, and ——, 2010b: Sensitivity of the simulated tropical cyclone inner-core size to the initial vortex size. *Mon. Wea. Rev.,* **138,** 4135–4157.

Zehr, R. M., 2003: Environmental wind shear with Hurricane Bertha. *Wea. Forecasting,* **18,** 345–356.

Zhou, X., and B. Wang, 2011: Mechanism of concentric eyewall replacement cycles and associated intensity change. *J. Atmos. Sci.,* **68,** 972–988.

Ziegler, C. L., W. J. Martin, R. A. Pielke, and R. L. Walko, 1995: A modeling study of the dryline. *J. Atmos. Sci.,* **52,** 263–285.